This is the preprint of the paper published in
INTERNATIONAL JOURNAL FOR NUMERICAL METHODS IN FLUIDS
Int. J. Numer. Meth. Fluids 2012; **69**:57–79

A fluid solver based on vorticity – helical density equations with application to a natural convection in a cubic cavity

Maxim A. Olshanskii*

Department of Mechanics and Mathematics, M. V. Lomonosov Moscow State University, Moscow 119899, Russia

SUMMARY

We study numerically a recently introduced formulation of incompressible Newtonian fluid equations in vorticity – helical density and velocity – Bernoulli pressure variables. Unlike most numerical methods based on vorticity equations, the current approach provides discrete solutions with mass conservation, divergence-free vorticity, and accurate kinetic energy balance in a simple and natural way. The method is applied to compute buoyancy-driven flows in a differentially heated cubical enclosure in the Boussinesq approximation for $Ra \in \{10^4, 10^5, 10^6\}$. The numerical solutions on a finer grid are of benchmark quality. The computed helical density allows quantification of the three-dimensional nature of the flow. Copyright © 2012 John Wiley & Sons, Ltd.

KEY WORDS: The Navier-Stokes equations; vorticity; helicity; helical density; heat transfer; Linear solvers

1. INTRODUCTION

Numerical simulation of isothermal and buoyancy-driven incompressible flows is an important task in many industrial applications and remains within the focus of intensive research. Incompressible viscous flows of a Newtonian fluid are modeled by the system of the Navier-Stokes equations typically written in "primitive" (velocity– pressure–density) variables. In many application assuming constant density is reasonable and leads to simpler models, such as Boussinesq approximation for natural convection problems. A popular numerical approach for such models utilizes the velocity-vorticity form of the Navier-Stokes equations. In three dimensions, the vorticity equations, resulting from the formal application of $\nabla\times$ to the momentum equations, can be written as

$$\frac{\partial \mathbf{w}}{\partial t} - \nu\Delta\mathbf{w} + (\mathbf{u}\cdot\nabla)\mathbf{w} - (\mathbf{w}\cdot\nabla)\mathbf{u} = \nabla\times\mathbf{f} \tag{1}$$

where $\mathbf{w} = \nabla\times\mathbf{u}$ is the flow vorticity. The volume forces $\mathbf{f}$ may include buoyancy force. The vorticity equations are typically complemented with the vector Poisson equation linking velocity and vorticity

$$-\Delta\mathbf{u} = \nabla\times\mathbf{w} \tag{2}$$

and possibly the convection-diffusion temperature equation. The first application of vorticity equations in CFD may be traced back to the late 70's [9]; the review paper of [11] summarizes many aspects of the approach; see also [15, 17, 24, 23] for more recent applications of velocity – vorticity

*Correspondence to: Department of Mechanics and Mathematics, M. V. Lomonosov Moscow State University, Vorobievy gory 1, Moscow 119899, Russia; Maxim.Olshanskii@mtu-net.ru

Contract/grant sponsor: Partially supported by the Russian Academy of Science program "Contemporary problems of theoretical mathematics" through the project No. 01.2.00104588 and RFBR Grants 09-01-00115 and 11-01-00767

formulation to both isothermal and buoyancy-driven flows. The advantages of using the vorticity Equation (1) for numerical simulations include the following: it allows access of the physically relevant variables of vortex dominated flows, simpler elliptic operators arise rather than the saddle-point problems because the pressure term is eliminated, and boundary conditions can be easier to implement in external flows where the vorticity at infinity is easier to set than the pressure boundary condition. In particular, in the finite element context, the vorticity-velocity formulation produces a vorticity field that is globally continuous. This is unlike the velocity-pressure formulation for most common element choices.

At the same time, using the Equations (1)–(2) for computations has some issues. First, one has to supply $\mathbf{w}$ and $\mathbf{u}$ with some boundary conditions to recover divergence free velocity and vorticity. On the differential level the question can be reformulated as looking for boundary conditions which ensure the formal (i.e. assuming $\mathbf{w}$ and $\mathbf{u}$ are smooth enough) equivalence of (1)–(2) to the primitive variable formulation. One example of such conditions for enclosed flows is setting

$$\begin{cases} \mathbf{u} = g \\ \mathbf{w} \times \mathbf{n} = (\nabla \times \mathbf{u}) \times \mathbf{n} \qquad \text{on } \partial\Omega, \\ \operatorname{div} \mathbf{w} = 0 \end{cases} \tag{3}$$

where $\mathbf{n}$ is the outward normal vector for $\partial\Omega$. However, the question remains open of what can be said about mass and $\operatorname{div} \mathbf{w} = 0$ conservation for *discrete* solutions. Thus, setting proper boundary or integral conditions for (1) and (2) is a controversial subject discussed in many publications, see e.g. [7, 11, 15, 20, 22, 23] and references therein. Furthermore, there is virtually no mathematical analysis of numerical schemes in velocity – vorticity variables. This is in contrast to the primitive variable schemes, which enjoy nowadays a solid mathematical foundation, including error analysis (one may consult a classical text [12] in a body of literature on the subject). A possible reason for such a situation is that the energy balance

$$\frac{1}{2}\int_\Omega |\mathbf{u}(t)|^2 + \nu \int_0^t \int_\Omega |\nabla \mathbf{u}|^2 = \frac{1}{2}\int_\Omega |\mathbf{u}(0)|^2 + \int_0^t \int_\Omega \mathbf{f} \cdot \mathbf{u}, \tag{4}$$

which easily follows from the momentum equation provided $\mathbf{u} = \mathbf{0}$ on the boundary of a bounded domain Ω, can be shown for the solution of (1)–(3) if one resorts back to the equivalent primitive variable formulation. Such an equivalence does not hold for *discrete* solutions, leading to the unclear situation with the validity of the discrete counterpart of (4) for numerical solutions to (1)–(3). We recall that (4) is fundamental for stability analysis.

We address the issues of the velocity-vorticity method (1)–(3) by (first) reformulating the vorticity equation as (to check the equivalence one has to use $\operatorname{div} \mathbf{u} = \operatorname{div} \mathbf{w} = 0$, cf. [19])

$$\frac{\partial \mathbf{w}}{\partial t} - \nu \Delta \mathbf{w} + 2\mathbb{D}(\mathbf{w})\mathbf{u} - \nabla(\mathbf{u} \cdot \mathbf{w}) = \nabla \times \mathbf{f}. \tag{5}$$

with $\mathbb{D}(\mathbf{w}) := \frac{1}{2}(\nabla \mathbf{w} + [\nabla \mathbf{w}]^T)$. The scalar product of velocity and vorticity appearing as the potential term has the physical meaning of the helical density $\eta := \mathbf{u} \cdot \mathbf{w}$. If the helical density is treated as an independent variable, it acts as a Lagrange multiplier corresponding to the div-free condition for vorticity. In this way, (5) is supplemented with the equation

$$\operatorname{div} \mathbf{w} = 0.$$

The helical density η is related to the helicity by $H = \int_\Omega \eta \, d\mathbf{x}$. The helicity H is a fundamental quantity in laminar and turbulent flow: it can be interpreted physically as the degree to which a flow's vortex lines are tangled and intertwined (defined precisely in terms of the total circulation and Gauss linking number of interlocking vortex filaments), is an inviscid invariant, cascades over the inertial range jointly with kinetic energy, manifests the lack of reflectional symmetry of a flow, and is believed to be closely related to vortex breakdown [1, 2, 6, 16].

If the helical density is identically zero, then, in a certain sense, the flow resembles the two-dimension geometric situation, when the vorticity vector has only one non-zero component

DOI: 10.1002/fld

orthogonal to the flow plane. Recently under similar conditions the regularity of the three-dimension Navier-Stokes solutions with arbitrary large data was established in [3]. Thus, the deviation of η from zero can be used to quantify the three dimensional nature of the flow. Moreover, that helicity is an inviscid invariant and is precisely balanced in the forced viscous case means that computed solutions' helicity can be used as a further diagnostic check for physical accuracy. Thus the formulation of Navier-Stokes equations studied here might give another insight into the vorticity dynamics and flow topology, and leads to numerical methods which directly approximate and access such physically important variables as vorticity and helicity.

We consider the vorticity-helical density equations:

$$\begin{cases} \dfrac{\partial \mathbf{w}}{\partial t} - \nu\Delta\mathbf{w} + 2\mathbb{D}(\mathbf{w})\mathbf{u} - \nabla\eta = \nabla\times\mathbf{f}, \\ \operatorname{div}\mathbf{w} = 0. \end{cases} \tag{6}$$

Some equations linking velocity and vorticity still have to be added to the system. Instead of vector Poisson equations (2) we consider the momentum equations with non-linear terms written in the rotation form:

$$\begin{cases} \dfrac{\partial \mathbf{u}}{\partial t} - \nu\Delta\mathbf{u} + \mathbf{w}\times\mathbf{u} + \nabla P = \mathbf{f}, \\ \operatorname{div}\mathbf{u} = 0, \\ \mathbf{u}|_{t=0} = \mathbf{u}_0 \end{cases} \tag{7}$$

where $P = \frac{1}{2}|\mathbf{u}|^2 + p$ is the Bernoulli pressure variable. Such a choice gives several benefits discussed below. The formulation (6)–(7) was first suggested in [19] and named the VVH (velocity-vorticity-helicity) form of the Navier-Stokes equations. It was shown that for smooth solutions the VVH and the primitive variable forms are equivalent with a simple and natural choice of the vorticity-helical density boundary conditions:

$$\mathbf{w} = \nabla\times\mathbf{u} \quad \text{on } \partial\Omega \tag{8}$$

or

$$\eta = \mathbf{u}\cdot(\nabla\times\mathbf{u}) \quad \text{and} \quad \mathbf{n}\times\mathbf{w} = \mathbf{n}\times(\nabla\times\mathbf{u}) \quad \text{on } \partial\Omega. \tag{9}$$

Although the VVH form involves twice as many unknowns as the primitive variable form, its advantages include the following:

- Numerical methods for (6)– (7) solve directly for important inviscid invariants η, P as well as for vorticity;
- The mass conservation and $\operatorname{div}\mathbf{w} = 0$ are enforced explicitly independent of boundary conditions. The accuracy of $\operatorname{div}\mathbf{u} = 0$ and $\operatorname{div}\mathbf{w} = 0$ enforcement depends only on the numerical method of choice. In particular, local mass conservation can be achieved using finite elements with discontinuous pressure approximations;
- The Lamb vector $\mathbf{w}\times\mathbf{u}$ from (7) is orthogonal to $\mathbf{u}$. Thus, multiplying the momentum equations from (7) by $\mathbf{u}$ and integrating over Ω and a time interval, immediately gives the energy balance relation (4). Similar consideration is true for many discretizations of (7), for example by a finite element method. This enables the first numerical analysis of a vorticity based method, see [14];
- If $\mathbf{u}$ is 'freezed', then (6) is linear with respect to the vorticity variable; and vice versa, if $\mathbf{w}$ is 'freezed', then (7) is linear with respect to the velocity variable. This suggests a natural splitting time-stepping algorithm which was numerically shown in [19] to possess excellent stability and accuracy.

The paper studies the numerical performance of the VVH formulation applied to compute a buoyancy-driven flow in a differentially heated cubical enclosure. We present quasi-time-stepping scheme and iterative methods to solve the systems of linear equations resulting from the finite-difference discretization of (6)–(8). It is shown that the Lagrange multiplier η does converge to the physical helical density, which is then used to quantify the three-dimensional nature of the flow.

DOI: 10.1002/fld

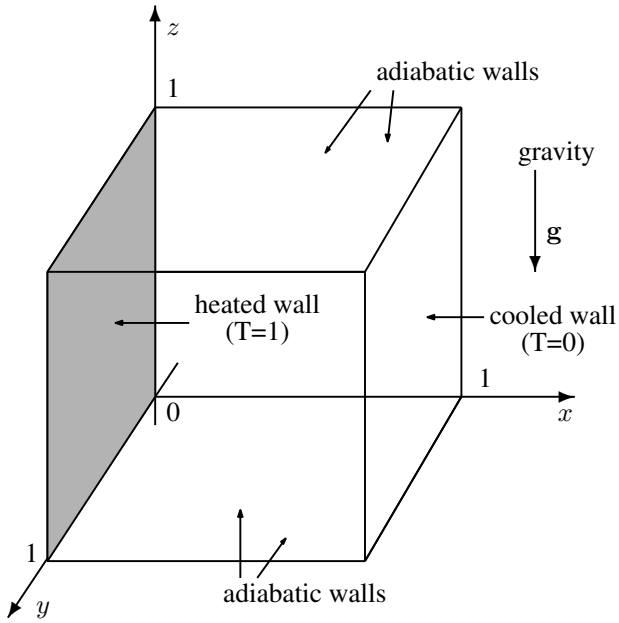

Figure 1. Schematic setup of the natural convection in a cubic cavity problem.

The rest of the paper is organized as follows. Section 2 gives the details of the test problem setup and of a second order finite-difference discretization method on semi-staggered grids. A quasi-time-stepping scheme and iterative method are considered in Section 3. Section 4 presents the results of numerical experiments.

2. THE PROBLEM SETUP AND DISCRETIZATION

Consider the unit cube $\Omega = (0,1)^3$ filled with a fluid. All six walls are assumed to be rigid and impermeable. The vertical walls located at $x = 0$ and $x = 1$ are retained isothermal at temperatures $T|_{x=0} = 1$ and $T|_{x=1} = 0$, respectively. The remaining four walls are adiabatic. The buoyancy force due to the gravity works in the negative z direction. The problem setup is shown schematically in Fig. 1.

We are interested in the equilibrium flow of incompressible viscous fluid in the Boussinesq approximation. The dimensionless form of the governing equations in primitive variables reads: Solve for steady state velocity $\mathbf{u}$, pressure p and temperature T

$$\begin{cases} -\dfrac{1}{Re}\Delta\mathbf{u} + (\mathbf{u}\cdot\nabla)\mathbf{u} + \nabla p = \dfrac{Gr}{Re^2}T\mathbf{g} \\ \operatorname{div}\mathbf{u} = 0 \\ -\dfrac{1}{Re\,Pr}\Delta T + (\mathbf{u}\cdot\nabla)T = 0 \end{cases} \quad \text{in } \Omega,$$

subject to boundary conditions

$$\mathbf{u} = \mathbf{0} \quad \text{on } \partial\Omega, \quad T|_{x=0} = 1, \; T|_{x=1} = 0, \; \frac{\partial T}{\partial \mathbf{n}}|_{y=\{0,1\}\cup z=\{0,1\}} = 0. \tag{10}$$

where Re, Pr and Gr are dimensionless Reynolds, Prandtl and Grashof numbers. To facilitate comparison with benchmark results found in the literature, we set $Gr = Re^2$ and $Pr = 0.71$, then the problem similarities are governed by the single non-dimensional Rayleigh number $Ra = Re^2 Pr$.

DOI: 10.1002/fld

In the paper we consider the following equivalent VVH formulation: Solve for steady state velocity $\mathbf{u}$, Bernoulli pressure P, vorticity $\mathbf{w}$, helical density η and temperature T (we simplify using $Gr = Re^2$):

$$\begin{cases} -\dfrac{1}{Re}\Delta\mathbf{u} + \mathbf{w}\times\mathbf{u} + \nabla P = T\mathbf{g} \\ -\dfrac{1}{Re}\Delta\mathbf{w} + 2\mathbb{D}(\mathbf{w})\mathbf{u} - \nabla\eta = \nabla\times(T\mathbf{g}) \\ \operatorname{div}\mathbf{u} = \operatorname{div}\mathbf{w} = 0 \\ -\dfrac{1}{Re\,Pr}\Delta T + (\mathbf{u}\cdot\nabla)T = 0 \end{cases} \quad \text{in } \Omega, \tag{11}$$

satisfying boundary conditions (10) and

$$\mathbf{w} = \nabla\times\mathbf{u} \quad \text{on } \partial\Omega. \tag{12}$$

2.1. Discretization method

We use a second order finite difference (FD) method based on a uniform cubic grid. Velocity, vorticity and temperature variables are located in vertices, while pressure and helical density are approximated in the centers of cubic volumes. This semi-staggered approximation is convenient for (11) due to the co-location of all velocity and vorticity components, however it suffers from the well-known "checkerboard mode" type instability (e.g., [4], p. 244) and has to be stabilized accordingly. For primitive variable equations the appropriate stabilization and the analysis of the scheme is given in [18]. Below we outline the discretization method.

The Laplace operator is approximated using the standard 7-point stencil; streamline derivatives in vorticity and temperature equations are discretized by the second-order upwind differences, with the exception of next to boundary nodes where first order upwind approximation is applied. Due to the collocation of velocity and vorticity variables, the straightforward approximation of the Lamb vector:

$$(\mathbf{u}\times\mathbf{w})_{ijk} := \mathbf{u}_{ijk}\times\mathbf{w}_{ijk}$$

gives a skew-symmetric term and hence the discrete analog of the energy equality (4) is valid.

Vorticity boundary conditions from (12) are enforced in boundary nodes by approximating the normal derivatives in $\nabla\times\mathbf{u}$ by second order one-side differences, for example

$$\mathbf{w}^2_{0jk} = (-3\mathbf{u}^3_{0jk} + 4\mathbf{u}^3_{1jk} - \mathbf{u}^3_{2jk})/(2h_x)$$

where $\mathbf{v}^k$ denotes the kth component of a vector function $\mathbf{v}$. Note that the tangential derivatives of velocity vanish on $\partial\Omega$. The same second order one-side difference formula was used to approximate adiabatic boundary condition from (10). All other operators, including the stretching term $(\nabla\mathbf{w})^T\mathbf{u}$ in $\mathbb{D}(\mathbf{w})\mathbf{u}$ from (11), were discretized by standard central differences.

To filter out unstable pressure (and helicity) modes the discrete divergence constraints in (10) are penalized. For example the discrete incompressibility equation reads

$$\operatorname{div}_h\mathbf{u}_h + G_h P_h = 0 \tag{13}$$

with a linear stabilization difference operator G_h acting on discrete pressures (Bernoulli pressures in our case). The operator G_h can be defined in several ways. For example, mimicking the finite element method from [5] one may define G_h through

$$G_h = -\alpha h^2\Delta_h, \tag{14}$$

where Δ_h is the usual 7-point approximation of the Laplace operator with the Neumann boundary conditions imposed in fictitious pressure nodes. A different choice of the filtering operator G_h is studied in [18]. We found that for the given problem both choices lead to very similar results. One has to chose a parameter α and a 'characteristic' mesh parameter h. We set $\alpha = 0.25$ for the incompressibility equation and $\alpha = 1$ to stabilize discrete helical density. These values of α were experimentally found to be close to optimal ones in the sense that notably smaller α-s lead to unstable discrete pressure or helical density, respectively.

DOI: 10.1002/fld

3. ITERATIVE SOLVERS

The quasi-time-stepping fully implicit method is used to converge to the steady state solution of the VVH system: Given the initial guess $\mathbf{u}^0, \mathbf{w}^0, T^0$ compute for $n = 0, 1, \dots$ until convergence:

$$\begin{aligned} -\Delta\frac{\mathbf{u}^{n+1}-\mathbf{u}^n}{\tau} - \frac{1}{Re}\Delta\mathbf{u}^{n+1} + \mathbf{w}^{n+1}\times\mathbf{u}^{n+1} + \nabla P^{n+1} &= T^{n+1}\mathbf{g},\\ -\Delta\frac{\mathbf{w}^{n+1}-\mathbf{w}^n}{\tau} - \frac{1}{Re}\Delta\mathbf{w}^{n+1} + 2\mathbb{D}(\mathbf{w}^{n+1})\mathbf{u}^{n+1} - \nabla\eta^{n+1} &= \nabla\times(T^{n+1}\mathbf{g}),\\ \operatorname{div}\mathbf{u}^{n+1} = \operatorname{div}\mathbf{w}^{n+1} &= 0,\\ -\Delta\frac{T^{n+1}-T^n}{\tau} - \frac{1}{Re\,Pr}\Delta T^{n+1} + (\mathbf{u}^{n+1}\cdot\nabla)T^{n+1} &= 0, \end{aligned} \tag{15}$$

where $\mathbf{u}^{n+1}$, $\mathbf{w}^{n+1}$, T^{n+1} satisfy boundary conditions (10) – (12). The stopping criteria was the fulfilment of the following inequality:

$$\left(\left\|\frac{\mathbf{u}^{n+1}-\mathbf{u}^n}{\tau}\right\|^2 + \left\|\frac{\mathbf{w}^{n+1}-\mathbf{w}^n}{\tau}\right\|^2 + \left\|\frac{T^{n+1}-T^n}{\tau}\right\|^2\right)^{\frac{1}{2}} \le 1e-6.$$

Here and further $\|\phi\|$ denotes the (discrete) L^2-norm, e.g. $\|\phi\|^2 = \sum_{\text{all nodes } \mathbf{x}_i} h^3\phi^2(\mathbf{x}_i)$.

On every pseudo-time step of (15) a nonlinear problem has to be solved. This problem is of the same type as the original one, but involves larger "effective" numerical viscosity coefficients:

$$\nu_t := \frac{1}{\tau} + \frac{1}{Re} \quad \text{and} \quad \mu_t := \frac{1}{\tau} + \frac{1}{Re\,Pr}.$$

We use $\tau = 25$ in all experiments. Therefore $\nu_t, \mu_t > 0.04$ and Picard or Newton iterations converge fast and almost independent of the original problem Rayleigh number. We apply the Picard type iterations given below. Set $\mathbf{w}_0 = \mathbf{w}^n$, $T_0 = T^n$ and compute for $k = 0, 1, \dots$ until convergence:

$$\text{Step 1:} \quad \begin{cases} -\nu_t\Delta\mathbf{u}_{k+1} + \mathbf{w}_k\times\mathbf{u}_{k+1} + \nabla P_{k+1} = T_k\mathbf{g},\\ \operatorname{div}\mathbf{u}_{k+1} = 0. \end{cases} \tag{16}$$

$$\text{Step 2:} \quad -\mu_t\Delta T_{k+1} + (\mathbf{u}_{k+1}\cdot\nabla)T_{k+1} = 0, \tag{17}$$

$$\text{Step 3:} \quad \begin{cases} -\nu_t\Delta\mathbf{w}_{k+1} + 2\mathbb{D}(\mathbf{w}_{k+1})\mathbf{u}_{k+1} - \nabla\eta_{k+1} = \nabla\times(T_{k+1}\mathbf{g}),\\ \operatorname{div}\mathbf{w}_{k+1} = 0. \end{cases} \tag{18}$$

where $\mathbf{u}^{k+1}$, $\mathbf{w}^{k+1}$, T^{k+1} satisfy boundary conditions (10) – (12). The iteration (16)–(18) was stopped once the ℓ_2-norm of the nonlinear residual has been reduced by 2 orders. More stringent convergence criteria did not lead to a faster convergence of (15) towards equilibrium.

Ra	$N_{(15)}$	N_{Picard}	$N_{(16)}$	$N_{(17)}$	$N_{(18)}$
1e+4	89	1.17	5.88	5.76	6.17
1e+5	284	1.06	4.86	4.93	4.99
1e+6	998	1.00	4.30	4.41	3.53

Table I. $N_{(15)}$ is the total number of pseudo-time steps in (15); N_{Picard} is the average number of the Picard iterations (16)–(18) on one time step; $N_{(16)}$, $N_{(17)}$, $N_{(18)}$ are the average numbers of the BiCGstab iterations for solving (16), (17), and (18), respectively, on every Picard iteration.

On each step of (16)–(18), a linear system of equations has to be solved. These were solved approximately with the help of preconditioned BiCGstab iterations. One V(2,2)-cycle of geometric multigrid (see, e.g., [13]) for Poisson problem was used as a preconditioner for solving the

DOI: 10.1002/fld

Ra	Method	$\psi_2(\mathbf{x}_c)$	$w_2(\mathbf{x}_c)$	$\max u_1$ ($z_{\max}$)	$\max u_3$ ($x_{\max}$)
1e+4	present($\frac{1}{32}$)	0.05403	1.1000	0.1971 (0.825)	0.2204 (0.117)
	present($\frac{1}{64}$)	0.05462	1.0935	0.1979 (0.826)	0.2211 (0.116)
	present($\frac{1}{128}$)	0.05471	1.0997	0.1981 (0.826)	0.2211 (0.116)
	[24]	0.05492	1.1018	0.1984 (0.825)	0.2216 (0.117)
	[21]			0.1984 (0.824)	0.2252 (0.120)
	[10]			0.2013 (0.817)	0.2252 (0.117)
1e+5	present($\frac{1}{32}$)	0.03299	0.1414	0.1395 (0.851)	0.2425 (0.0664)
	present($\frac{1}{64}$)	0.03367	0.2340	0.1409 (0.853)	0.2448 (0.0646)
	present($\frac{1}{128}$)	0.03382	0.2513	0.1412 (0.853)	0.2453 (0.0641)
	[24]	0.03406	0.2576	0.1416 (0.850)	0.2461 (0.0667)
	[21]			0.1410 (0.854)	0.2447 (0.0670)
	[10]			0.1468 (0.855)	0.2471 (0.0647)
1e+6	present($\frac{1}{32}$)	0.01876	0.0909	0.0639 (0.654)	0.2674 (0.0399)
	present($\frac{1}{64}$)	0.01994	0.1446	0.0765 (0.842)	0.2566 (0.0373)
	present($\frac{1}{128}$)	0.01964	0.1324	0.0799 (0.854)	0.2567 (0.0376)
	[24]	0.01979	0.1366	0.0811 (0.858)	0.2587 (0.0333)
	[21]			0.0810 (0.854)	0.2582 (0.0331)
	[10]			0.0842 (0.856)	0.2588 (0.0331)

Table II. Reference and computed values of maximum centerlines velocities, y-components of vorticity and stream function values.

convection-diffusion problem in (17), and the 2x2 block-triangle (left) preconditioner of the form

$$\begin{pmatrix} -\nu_t L & 0 \\ B & -\nu_t^{-1} I \end{pmatrix}^{-1}$$

as a preconditioner for saddle point problems on steps (16) and (18). Here L^{-1} is again the one V(2,2)-cycle of geometric multigrid for the vector Poisson problem, B is the matrix of the discrete divergence operator and I is the identity matrix of a dimension equal to the dimension of the discrete pressure (or helical density) space. For the analysis of block-triangle preconditioners for the saddle-point problems see [8] and references therein. The stopping stopping criteria for the BiCGstab iterations was the reduction of the residual by the factor of 10^2. The performance of (15), (16)–(18) and the linear solvers are summarized in Table I for different values of the Rayleigh number and mesh size $= \frac{1}{32}$. With decreasing the mesh sizes (we computed also with mesh sizes $\frac{1}{64}, \frac{1}{128}$) the number of iterations and pseudo-time steps were about the same or slightly decreasing. Thus the entire approach scales optimally with respect to the number of unknowns. Finally, we remark that the ad hoc value of the pseudo-time step $\tau = 25$ nearly compromises between the convergence of Picard and linear iterations (faster for smaller τ) and the tendency of the solution towards the equilibrium state (faster for larger τ).

4. NUMERICAL RESULTS

We compute solutions to (11),(10), (12) on the sequence of uniformly refined meshes with mesh sizes $\in \{\frac{1}{32}, \frac{1}{64}, \frac{1}{128}\}$. Several statistics defined below are of common interest. First, the stream function can be introduced as a solution to the Poisson equation

$$\Delta \boldsymbol{\psi} = \nabla \times \mathbf{u} \ \text{ in } \ \Omega, \qquad \boldsymbol{\psi} \times \mathbf{n} = 0 \ \text{ and } \ \frac{(\partial \boldsymbol{\psi} \cdot \mathbf{n})}{\partial \mathbf{n}} = 0 \ \text{ in } \ \partial\Omega. \tag{19}$$

The averaged Nusselt number for the constant x-plane is defined as

$$Nu(x) = \int_0^1 \int_0^1 (PrRe\, u_1 T - \frac{\partial T}{\partial x}) \mathrm{d}y \mathrm{d}z.$$

DOI: 10.1002/fld

Ra	Method	$S(\mathbf{x}_c)$	$Nu(\frac{1}{2})$	$Nu(0)$
1e+4	present($\frac{1}{32}$)	0.8586	2.085	2.030
	present($\frac{1}{64}$)	0.8615	2.063	2.048
	present($\frac{1}{128}$)	0.8619	2.057	2.053
	[24]	0.8634	2.0636	2.0624
	[21]		2.250	2.054
	[10]			2.100
1e+5	present($\frac{1}{32}$)	1.138	4.480	4.206
	present($\frac{1}{64}$)	1.092	4.369	4.306
	present($\frac{1}{128}$)	1.085	4.344	4.330
	[24]	1.087	4.3648	4.3665
	[21]		4.612	4.337
	[10]			4.361
1e+6	present($\frac{1}{32}$)	1.358	9.032	7.622
	present($\frac{1}{64}$)	0.969	8.813	8.454
	present($\frac{1}{128}$)	0.914	8.672	8.606
	[24]	0.9192	8.7097	8.6973
	[21]		8.877	8.640
	[10]			8.770

Table III. Reference and computed values of the stratification factor in the cavity center $\mathbf{x}_c$ and average Nusselt number for $x = \frac{1}{2}$ and $x = 0$ planes.

Ra	1e+4			1e+5			1e+6		
Mesh size	$\frac{1}{32}$	$\frac{1}{64}$	$\frac{1}{128}$	$\frac{1}{32}$	$\frac{1}{64}$	$\frac{1}{128}$	$\frac{1}{32}$	$\frac{1}{64}$	$\frac{1}{128}$
$\|\mathbf{w} - \nabla \times \mathbf{u}\|$	0.0560	0.0163	0.0045	0.2412	0.0688	0.0186	1.1455	0.3173	0.0823
$\|\mathbf{w} \cdot \mathbf{u} - \eta\|$	8.01e-3	2.29e-3	7.72e-4	2.14e-2	4.89e-3	1.30e-3	8.90e-2	1.97e-2	4.23e-3

Table IV. Convergence of computed variables.

The stratification factor in $\mathbf{x} \in \Omega$ is defined as $S(\mathbf{x}) = \frac{\partial T}{\partial z}(\mathbf{x})$. For the purpose of comparison with a data available in the literature we look for the values of $\psi_2(\mathbf{x}_c)$, $w_2(\mathbf{x}_c)$ and $S(\mathbf{x}_c)$ at the center of the cavity $\mathbf{x}_c = (0.5, 0.5, 0.5)$, and the averaged Nusselt number for the midplane at $x = 0.5$ and the heated wall at $x = 0$, as well as for maximum values of $u_1(0.5, 0.5, z)$ and $u_3(x, 0.5, 0.5)$. The computed fluid statistics are collected in Table II and the computed averaged Nusselt numbers and stratification factor are shown in Table III. The stream function was computed using discrete vorticity $\mathbf{w}$ in the right-hand side of (19). For comparison we use the reference values from [24], which have been computed using a 4th-order finite-difference scheme for the usual velocity-vorticity formulation on a sequence of meshes with the finest 120x120x120 mesh followed by the Richardson extrapolation. We also compare to values from [21] computed using a pseudo-spectral Chebyshev method for primitive variable formulation on a 81x81x81 mesh and the earlier results of Fusegi et al. [10]. Although there is some discrepancy in the 'reference' values from different sources, especially for higher Ra numbers, the statistics computed with the VVH scheme converge well within the range of reference data.

An additional accuracy indicator is the difference between the computed vorticity and the rotation of the computed velocity, as well as the difference between the computed helical density and the scalar product of the computed velocity and vorticity. The discrete L^2 norms of this quantities are given in Table IV. A slightly less than second order of convergence is observed both for $\|\mathbf{w} - \nabla \times \mathbf{u}\|$ and $\|\mathbf{w} \cdot \mathbf{u} - \eta\|$.

Figure 2 shows equally distributed isotherms for xz-midplane and vorticity y-component isolines for xz-midplane; both for solution computed with mesh size equal $\frac{1}{64}$. The values for vorticity isolines are taken the same as in [24] and virtually the plots coincide with those from [24]. We note that our approach performs well for the case when vorticity experiences boundary layers, as well seen for $Ra = 1e + 6$. In Figure 3 we present the velocity projections on the midplanes of the cavity.

DOI: 10.1002/fld

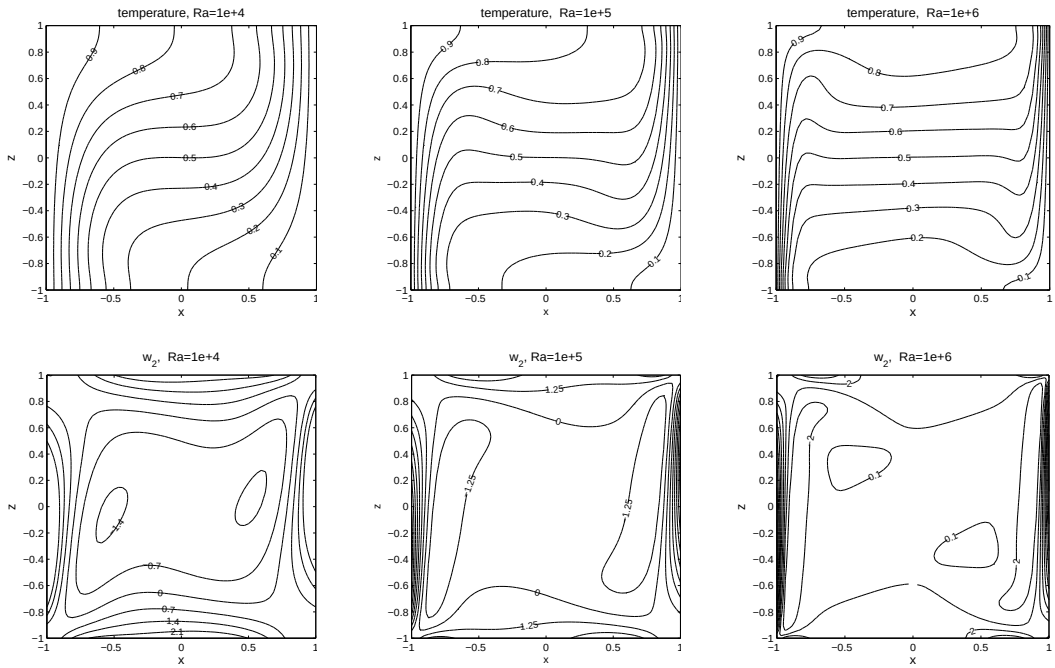

Figure 2. Top: Equally distributed isotherms for xz-midplane. Bottom: Vorticity w_2 isolines for xz-midplane equally distributed on [-1.4,4.9] for Ra=1e+4, on [-1.25,8.75] for Ra=1e+5, and on [-2,16] for Ra=1e+6.

Ra	1e+4	1e+5	1e+6
$\max_{\Omega} \lvert\eta\rvert$	5.24e-2	6.80e-2	1.26e-1
$\sqrt{\int_\Omega \eta^2 \lvert\mathbf{w}\rvert^{-2}\lvert\mathbf{u}\rvert^{-2}}$	1.83e-1	1.92e-1	2.38e-1

Table V. Maximum helical density and the integral norm of the normalized helical density.

One may note the increasing complexity of the flow pattern for higher Rayleigh numbers through the disjunction of the main recirculation zone into two and the formation of stronger corner vortices.

More insight into the flow structure can be gained by considering the helical density midplanes isolines in Figure 4 (in xz-midplane it holds $\eta = 0$). We recall that higher absolute values of the helical density manifest the local three-dimensional nature of the flow. Interesting to note that for higher Ra numbers and opposite to other variables η experiences boundary layers near the side adiabatic walls, where stronger helical fluid flow occurs, rather than near isothermal walls. Rather expecting, Table V shows the increase of the maximum absolute value of η as the Raleigh number grows.

Further, we note that the normalized helicity and the Lamb vector form the identity:

$$\frac{\eta^2}{|\mathbf{w}|^2|\mathbf{u}|^2} + \frac{|\mathbf{w}\times\mathbf{u}|^2}{|\mathbf{w}|^2|\mathbf{u}|^2} = 1. \tag{20}$$

The vanishing of any of two terms on the left-hand side of (20) indicates that (locally) the flow is in one of the two extreme regimes, which can be characterized as follows.

- $|\eta| = 0$: The flow can be interpreted as essentially two-dimensional;
- $|\mathbf{w}\times\mathbf{u}| = 0$: In velocity–Bernoulli pressure variables the flow is 'linear' (if the buoyancy effects are neglected, cf. (7)).

DOI: 10.1002/fld

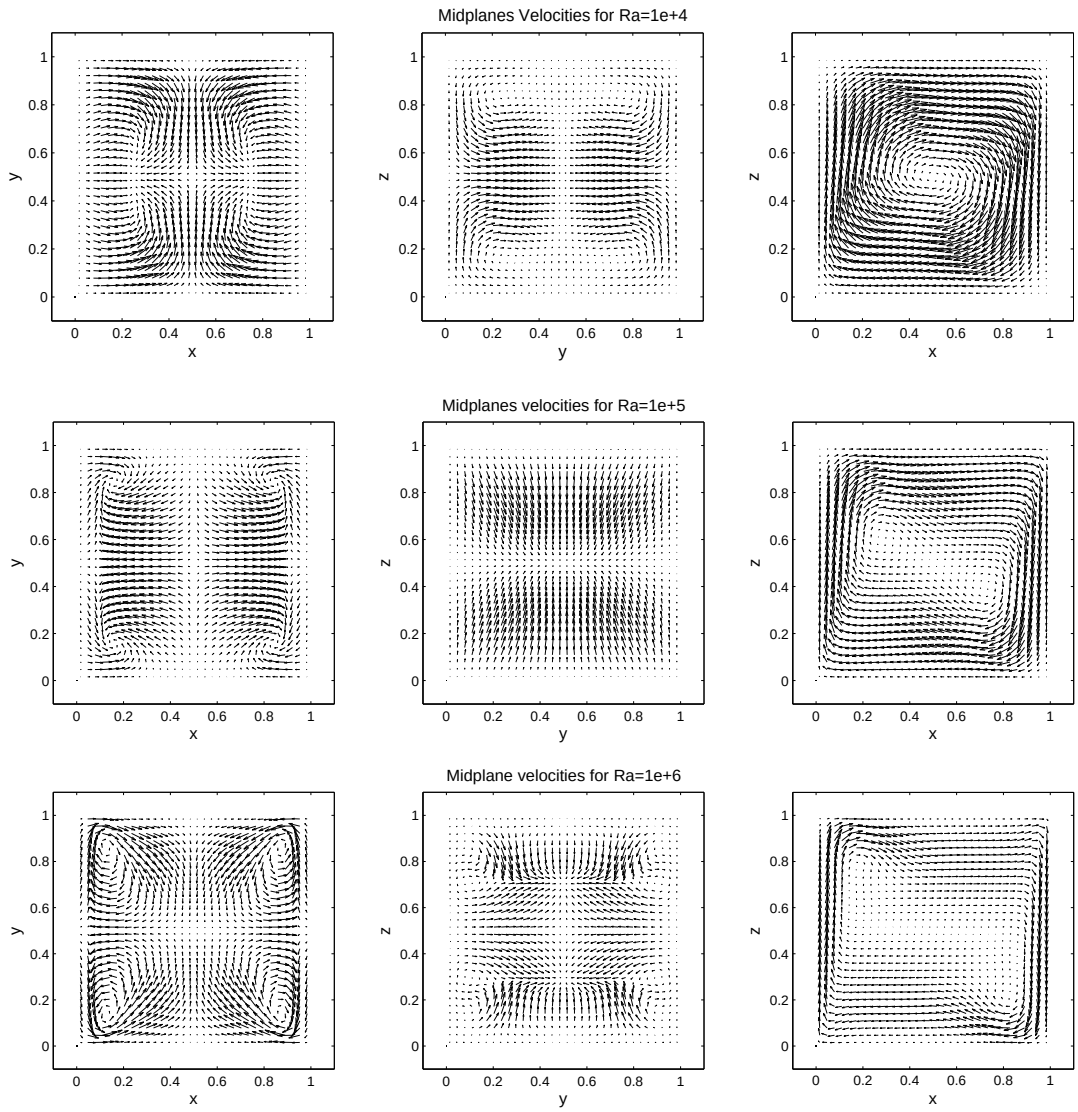

Figure 3. Steady state velocity fields at the midplanes.

It is clear that for fully developed unsteady flows most of fluid dynamics falls between these two extreme regimes.

To study the balance (20) for the buoyancy-driven steady flow in the heated cubical enclosure we introduce the following function $\mathcal{H}(\alpha)$ measuring the distribution of normalized helical density $|\eta||\mathbf{w}|^{-1}|\mathbf{u}|^{-1}$ values over the $[0,1]$ interval:

$$\mathcal{H}(\alpha) = \frac{\mathrm{d}H}{\mathrm{d}\alpha}, \quad \text{with } H(\alpha) := \mathrm{meas}(\Omega(\alpha)), \;\; \Omega(\alpha) := \left\{ \mathbf{x} \in \Omega \,:\, \frac{|\eta(\mathbf{x})|}{|\mathbf{w}(\mathbf{x})||\mathbf{u}(\mathbf{x})|} \le \alpha \right\},$$

where 'meas' denotes the three-dimension Lebesgue measure and assuming $H(\alpha)$ is differentiable. It holds

$$\int_0^1 \mathcal{H}(\alpha)\mathrm{d}\alpha = 1 \;\; (= \mathrm{meas}(\Omega)).$$

DOI: 10.1002/fld

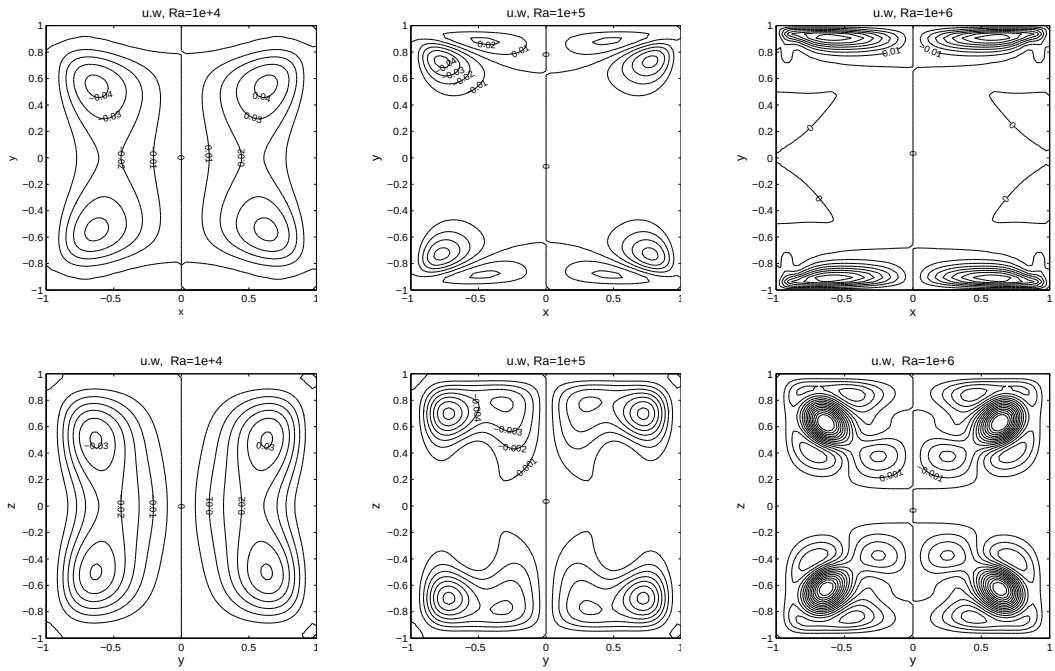

Figure 4. Top: Helical density isolines for xy-midplane equally distributed on [-0.04,0.04] for Ra=1e+4 and Ra=1e+5, and on [-0.07,0.07] for Ra=1e+6. Bottom: Helical density isolines for yz-midplane equally distributed on [-0.03,0.03] for Ra=1e+4, on [-0.007,0.007] for Ra=1e+5, and on [-0.01,0.01] for Ra=1e+6.

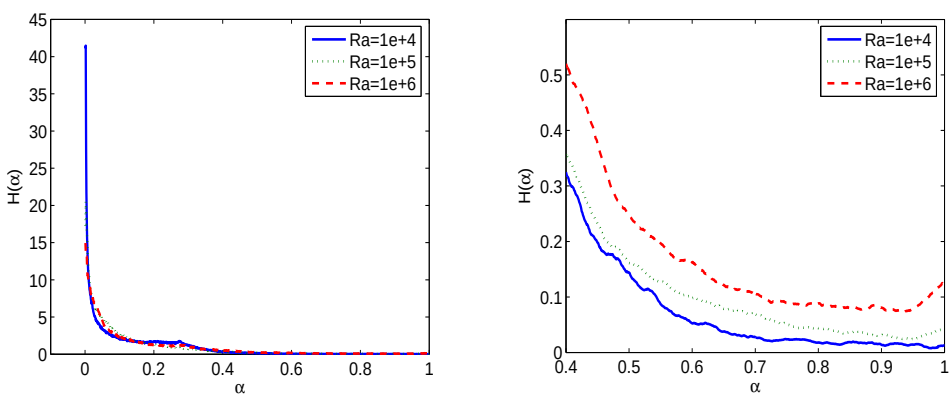

Figure 5. Normalized helical density distribution.

Function $\mathcal{H}$ can be interpret as the density of a distribution, where $\int_{\alpha_1}^{\alpha_2} \mathcal{H}(\alpha)$ measures what part of the domain is occupied by a fluid flowing with $\alpha_1 \leq |\eta||\mathbf{w}|^{-1}|\mathbf{u}|^{-1} \leq \alpha_2$.

The left plot in Figure 5 shows the graph of an approximation to $\mathcal{H}$ based on numerical solutions for three values of Rayleigh number. In the given scale all three graphs are very similar. From the plot it is clear that for the given Rayleigh numbers, the fluid dynamics is still close to two-dimensional in most parts of the domain and in the sense of (20) balance, see also Table V for the integral norm of the normalized helical density. The right picture in Figure 5 zooms the part of $\mathcal{H}$ plot for $\alpha \geq 0.4$ (here the graph of $\mathcal{H}$ was smoothed by averaging). The plot shows that the parts of

DOI: 10.1002/fld

the heated cube with flow of high normalized helicity are, however, not empty and are increasing for higher Rayleigh numbers.

REFERENCES

1. Andre JC, Lesieur M. Influence of helicity on the evolution of isotropic turbulence at high Reynolds number. *Journal of Fluid Mechanics* 1977; **81** : 187–207.
2. Arnold VI, Khesin BA. *Topological methods in hydrodynamics*. Series: Applied mathematical sciences. Springer: New York, 1998.
3. Berselli LC, Cordoba D. On the regularity of the solutions to the 3D Navier-Stokes equations: a remark on the role of the helicity. *Comptes Rendus Mathematique* 2009; **347** : 613–618.
4. Brezzi F, Fortin M. *Mixed and Hybrid Finite Element Methods*. Springer: New York, 1991.
5. Brezzi F, Pitkaranta J. On the stabilization of finite element approximations of the Stokes equations, in Efficient Solutions of Elliptic Systems. *Notes on Numerical Fluid Mechanics* 1984; **10** : 11–19.
6. Ditlevson P, Guiliani P. Cascades in helical turbulence. *Physical Review E* 2001; **63** : 036304.
7. Davies C, Carpenter PW. A Novel Velocity-Vorticity Formulation of the Navier-Stokes Equations with Applications to Boundary Layer Disturbance Evolution. *Journal of Computational Physics* 2001; **172** : 119–165.
8. Elman HC, Silvester DJ, Wathen AJ. *Finite Elements and Fast Iterative Solvers: with Applications in Incompressible Fluid Dynamics*. Numerical Mathematics and Scientific Computation. Oxford University Press: Oxford, 2005.
9. Fasel H. Investigation of the stability of boundary layers by a finite-difference model of the Navier-Stokes equations. *Journal of Fluid Mechanics* 1976; **78** : 355–383.
10. Fusegi T, Hyun JM, Kuwahara K, Farouk B. A numerical study of three-dimensional natural convection in a differentially heated cubical enclosure. *International Journal of Heat and Mass Transfer* 1991; **34** : 1543–1557.
11. Gatski TB. Review of incompressible fluid flow computations using the vorticity-velocity formulation. *Applied Numerical Mathematics* 1991; **7** : 227–239.
12. Girault V, Raviart PA. *Finite element methods for Navier-Stokes equations*. Springer: Berlin, 1986.
13. Hackbush W. *Multi-grid methods and applications*. Springer: Berlin, 1985.
14. Lee HK, Olshanskii MA, Rebholz LG. On error analysis for the 3D Navier-Stokes equations in Velocity-Vorticity-Helicity form. *SIAM Journal on Numerical Analysis* 2011; **49** : 711–732.
15. Lo DC, Young DL, Murugesan K. An accurate numerical solution algorithm for 3D velocity-vorticity Navier-Stokes equations by the DQ method, *Cmmunications in Numerical Methods in Engineering* 2006; **22** : 235–250.
16. Moffatt HK, Tsinober A. Helicity in laminar and turbulent flow. *Annual Review of Fluid Mechanics* 1992; **24** : 281–312.
17. Meitz HL, Fasel HF. A compact-difference scheme for the Navier-Stokes equations in vorticity-velocity formulation. *Journal of Computational Physics* 2000; **157** : 371–403.
18. Olshanskii MA. Analysis of semi-staggered finite-difference method with application to Bingham flows. *Computer Methods in Applied Mechanics and Engineering* 2009; **198** : 975–985.
19. Olshanskii MA, Rebholz LG. Velocity-Vorticity-Helicity formulation and a solver for the Navier-Stokes equations. *Journal of Computational Physics* 2010; **229** : 4291–4303.
20. Ruas V. A New Formulation of the Three-dimensional Velocity-Vorticity System in Viscous Incompressible Flow. *Zeitschrift für Angewandte Mathematik und Mechanik* 1999; **79** : 29–36.
21. Tric E, Labrosse G, Betrouni M. A first incursion into the 3D structure of natural convection of air in a differentially heated cubic cavity from accurate numerical solutions. *International Journal of Heat and Mass Transfer* 2000; **43** : 4043–4056.
22. Trujillo J, Karniadakis GE. A penalty method for the vorticity-velocity formulation. *Journal of Computational Physics* 1999; **149** : 32–58.
23. Wong KL, Baker AJ. A 3D incompressible Navier-Stokes velocity-vorticity weak form finite element algorithm. *International Journal for Numerical Methods in Fluids* 2002; **38** : 99–123.
24. Wakashima S, Saitoh TS. Benchmark solutions for natural convection in a cubic cavity using the high-order timespace method. *International Journal of Heat and Mass Transfer* 2004; **47** : 853–864.

DOI: 10.1002/fld